



THE 22ND CHESAPEAKE SAILING YACHT SYMPOSIUM

ANNAPOLIS, MARYLAND, MARCH 2016

Prediction and optimization of aerodynamic and hydrodynamic forces and boat speed of foiling catamarans with a wing sail and a jib

Kai Graf, University of Applied Sciences Kiel, Germany

Hannes Renzsch, Fluid Engineering Solutions GmbH, Schleswig, Germany

Janek Meyer, Yacht Research Unit Kiel, Germany

ABSTRACT

This paper describes a method to calculate the aerodynamic forces generated by a rigid two-element wing together with a jib. Additionally, investigations of hydrodynamic flow forces generated by water-piercing L-shaped foils are introduced. The aerodynamic and hydrodynamic flow force prediction methods are combined in a velocity prediction program featuring a constraint optimization method in order to predict boat speed and wing and foil trimming parameters for its maximization.

A velocity polar calculated by applying this method to a 50-foot catamaran is shown and the result of some studies are presented, varying design parameters of the catamaran.

NOTATION

CSYS	Chesapeake Sailing Yacht Symposium
A	Start point of vortex filament, $\mathbf{A}=\{x_A, y_A, z_A\}^T$
AoA	Angle of Attack (-)
A_{RW}	Area of rudder wing (m^2)
AWS	Apparent wind speed (m/s)
AWA	Apparent wind angle (-)
β, β_{flap}	Flap angle (-)
c	Profile Length (m)
c_D	Drag coefficient (-)
c_L	Lift coefficient (-)
D_{ind}	Induced drag (N)
D_{AX}, D_{AY}	Drag area in x- and y-direction (m^2)
ds	Integrator (m)
F_{AX}, F_{AY}	Windage force in x- and y-direction (N)
F	$=\{F_x, F_y, F_z\}^T$, global force (N)
L	Lift (N)
L	$ \mathbf{L} $ (N)
L_{VRW}	Vertical lift of rudder wing (N)
l, t	profile leading and trailing edge, $\mathbf{l}=\{x_l, y_l, z_l\}^T$
M	$=\{M_x, M_y, M_z\}^T$, global moment (Nm)

P	Collocation point, $\mathbf{P}=\{x_P, y_P, z_P\}^T$
R_I	Induced resistance (N)
R_T	Total resistance of hull (N)
R_{RW}	Resistance of rudder wing (N)
r	Vector from point to integrator ds (m)
r	$ \mathbf{r} $ (m)
s	vector along filament (m)
S_{RW}	Span of rudder wing (m)
s_{Eff}	Effective span (m)
T_{Eff}	Effective draft or span (m)
t/c	Jib profile depth over chord length (-)
u	Flow Velocity vector (m/s)
u_B	Boat speed
v	Induced Velocity vector (m/s)
v	Induced wind speed (m/s)
v_i	Induced wind speed at profile i (m/s)
v_j^*	Induced wind speed at panel j (m/s)
w_{FVF}	Lower free vortex filament weighting (-)
x, y, z	Coordinates in space (m)
y^+	Dimensionless wall distance (-)
z	Vertical span-wise coordinate (m)
z_{fvf}	Vertical coordinate of free vortex filament (m)
z_C	Vertical coordinate of the panel center (m)
z_I, z_2	Coordinates of lower and upper bound of wake sheet (m)
Δ	Displacement (kg)
λ	Aspect ratio of wing (-)
λ_{RW}	Aspect ratio of rudder wing (-)
Γ	Vorticity (m^2/s)
$\Delta\Gamma_{bound}$	Stepwise change of bound vorticity (m^2/s)
Γ_{bound}	Vorticity of bound vortex filament (m^2/s)
Γ_{fvf}	Vorticity of free vortex filament (m^2/s)
Γ_1, Γ_2	Vorticity at lower and upper bounds of wake sheet (m^2/s)
ρ, ρ_H	Density of air, density of water (kg/m^3)
ω	Relaxation factor (-)
SI units only	

INTRODUCTION

In a recent paper Graf et.al, 2014 published a method for the calculation of aerodynamic forces of rigid wings as they are used on modern racing catamarans, see Figure 1. The method is based on 2D-RANS investigations for the flow around wing profiles and a nonlinear lifting line method to account for three-dimensional flow phenomena. It has been combined with a constraint optimization method to find the trim of the wing for maximum driving forces and given heeling moment. This method successfully has been successfully applied to the AC 72 as well as the C-class catamaran wings.

This paper describes an enhancement of that method. It employs a lifting line method with multiple rather than single bound vortex filaments, thus allowing to take into account an additional jib, which is fully integrated into the trim optimization process. In addition the optimization procedure now is based on a maximization of boat speed rather than wing driving force. In order to do so, a hydrodynamic model for foiling catamarans has been added, taking into account an L-shaped, water surface piercing foils, which has been investigated using 3D-RANS free surface flow investigations. Rudders and hull windage is also taken into account.

The method is used to predict flow forces, boat speed and flying behavior of a 50 feet catamaran, similar to the yachts intended to be sailed in the next Americas Cup. It is used to predict a velocity polar for a range of wind speeds and true wind angles. Some parameter studies predict the impact of wing trim variations on the performance of the yacht.



Figure 1: Oracle Team USA in the 2013 America's Cup, Foto: Donan.Raven, License: CreativeCommons by-sa-3.0-de

AERODYNAMIC MODEL

Aerodynamic forces generated by the wing and the jib are calculated using a lifting line method. This method relies on lift and drag coefficients of the wing profiles and the jib, which are calculated by planar flow RANSE simulations.

Lifting Line Method

The lifting line method is based on the following principal: a bound vortex filament of piecewise linear, optionally discontinuous, vorticity distribution along span is running from root to tip of the wing. An additional bound vortex filament is located along the span of the jib, longitudinally in a point 1/4 of the profile length aft of the luff. Individual free vortex filaments and/or wake sheets (in any combination) are shedding from bound vortex filaments into infinity in the direction of incident flow, see Figure 2: Bound and free vortex filaments on a wing. Discrete vorticities of the free vortex filaments and the distributed vorticity per length of the wake sheet are calculated conforming to *Thompsons* rule, see Truckenbrodt, 1964. Induced wind is calculated from the free vortex filaments and the wake sheet using *Biot Savart's* law. Lift and induced drag is calculated from *Kutta's* law taking into account the sum of undisturbed flow velocity and induced wind. The discrete form of this method calculates the total drag as integration over span of the induced drag per span plus the viscous profile drag. In a similar manner, the profile lift is integrated over span, taking into account the local effective incident flow.

To take into account nonlinear lift coefficients with respect to angle of attack, in particular lift coefficient changes due to flow separation, an iterative approach is employed here. It is based on an iterative correction of induced wind from the spanwise lift distribution, which takes into account the induced wind as a correction of angle of attack.

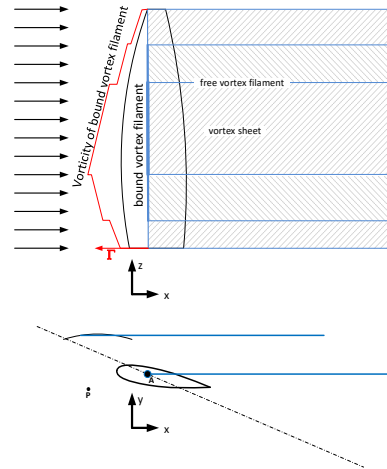


Figure 2: Bound and free vortex filaments on a wing

Theorems of *Kutta*, *Biot-Savart* and *Thompson* are used as follows:

Kutta's Law is used to calculate the lift generated by a vortex filament:

$$\mathbf{L} = \int_{span} \rho \mathbf{u} \Gamma \times d\mathbf{s} \quad (1)$$

where \mathbf{L} is the generated lift, ρ the density of flow, \mathbf{u} the incident flow, Γ the vorticity of filament and $d\mathbf{s}$ an integrator along the filament.

Biot-Savart's Law is used to calculate the induced wind generated by a vortex filament:

$$\mathbf{v} = \frac{-1}{4\pi} \int_s \Gamma \frac{\mathbf{r} \times d\mathbf{s}}{|\mathbf{r}|^3} \quad (2)$$

where \mathbf{v} is the induced velocity generated at $\mathbf{P} = \{x_p, y_p, z_p\}^T$ by the vortex filament of vorticity Γ . \mathbf{r} is a vector from \mathbf{P} to $\{x, y, z\}^T$, the current location of the integrator $d\mathbf{s}$ along the filament.

We assume that the span of the wing is oriented in z -direction of the coordinate system used and the incident velocity is directed parallel to the x -axis. A change of the angle of attack due to induced wind is then generated only by the y -component of the induced wind. This yield:

$$\mathbf{r} \times d\mathbf{s} = \begin{Bmatrix} x - x_p \\ y - y_p \\ z - z_p \end{Bmatrix} \times \begin{Bmatrix} dx \\ 0 \\ 0 \end{Bmatrix} = \begin{Bmatrix} 0 \\ (z - z_p)dx \\ -(y - y_p)dx \end{Bmatrix} \quad (3)$$

$$|\mathbf{r}|^3 = ((x - x_p)^2 + (y - y_p)^2 + (z - z_p)^2)^{3/2} \quad (4)$$

For the y -component of the induced velocity v we then get

$$v = \frac{-\Gamma}{4\pi} \int_s \frac{(z - z_p)dx}{((x - x_p)^2 + (y - y_p)^2 + (z - z_p)^2)^{3/2}} \quad (5)$$

Free vortex filaments are calculated by *Thompsons rule*, saying that a vortex filament may only end at a fixed wall or at infinity. *Prandtl's* concept of horseshoe vortices is used, saying that any change of the bound vortex filament results in a free vortex filament. This results in:

$$d\Gamma_{fif} = \frac{\partial \Gamma_{bound}(z)}{\partial z} dz \quad (6)$$

For a stepwise change of the vorticity of the bound vortex filament $\Delta \Gamma_{bound}$, the vorticity of the free vortex filament at the position of the stepwise change calculates from:

$$\Gamma_{fif} = \Delta \Gamma_{bound} \quad (7)$$

Generated from a stepwise change of Γ_{bound} at location $\mathbf{A} = \{x_A, y_A, z_A\}^T$ a free vortex filament of constant vorticity Γ_{fif} starts at \mathbf{A} and is running at constant y, z to $\{\infty, y_A, z_A\}^T$. It generates induced wind in $\mathbf{P} = \{x_p, y_p, z_p\}^T$ in the direction of the y -axis by (see Figure 3):

$$v = \frac{-\Delta \Gamma_{bound}(z_A - z_p)}{4\pi} \int_{x_A}^{\infty} \frac{dx}{((x - x_p)^2 + (y_A - y_p)^2 + (z_A - z_p)^2)^{3/2}} \quad (8)$$

Integration gives:

$$v = \frac{-\Delta \Gamma_{bound}}{4\pi} \frac{\Delta z}{\Delta y^2 + \Delta z^2} \left(1 - \frac{\Delta x}{(\Delta x^2 + \Delta y^2 + \Delta z^2)^{1/2}} \right) \quad (9)$$

with $\Delta x = x_A - x_p, \Delta y = y_A - y_p, \Delta z = z_A - z_p$ (9) holds for an infinite small vorticity $\partial \Gamma$ starting at $\{x_A, y_A, z\}^T$ to $\{\infty, y_A, z\}^T$, yielding:

$$v = \frac{-\partial \Gamma}{4\pi} \frac{z - z_p}{\Delta y^2 + (z - z_p)^2} \left(1 - \frac{\Delta x}{(\Delta x^2 + \Delta y^2 + (z - z_p)^2)^{1/2}} \right) \quad (10)$$

For a vortex sheet we assume a span-wise change of $\Gamma_{bound}(z)$, varying linearly between $\mathbf{A}_1 = \{x_A, y_A, z_1\}^T$ and $\mathbf{A}_2 = \{x_A, y_A, z_2\}^T$ from Γ_1 to Γ_2 :

$$\Gamma_{bound}(z) = \Gamma_1 + \frac{\Gamma_2 - \Gamma_1}{z_2 - z_1} (z - z_1) \quad (11)$$

Introducing (11) into (6) yields: $\partial \Gamma_{fif} = \frac{\Gamma_2 - \Gamma_1}{z_2 - z_1} dz$.

Introducing this into (10) and integrating from z_1 to z_2 yields:

$$v = -\frac{\Gamma_2 - \Gamma_1}{4\pi(z_2 - z_1)} \ln \left(\frac{\sqrt{(z_2 - z_p)^2 + \Delta y^2 + \Delta x^2} + \Delta x}{\sqrt{(z_1 - z_p)^2 + \Delta y^2 + \Delta x^2} + \Delta x} \right) \quad (12)$$

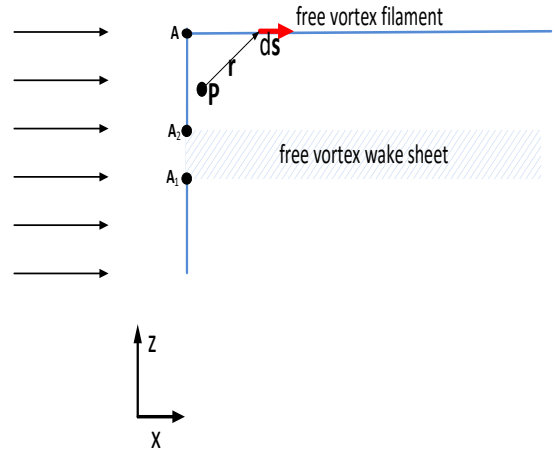


Figure 3: Free vortex filament and wake sheet, generating induced velocity at arbitrary point P

Profile lift per span length $L = d\mathbf{L}/dz$ is calculated from a lift coefficient c_L , the dynamic pressure $0.5\rho AWS^2$ and the profile chord length c . c_L depends nonlinear on angle of attack AoA of incident flow. For a profile of a wing of finite span the angle of attack is AoA reduced by induced wind:

$$L = 0.5\rho AWS^2 c - c_L(AoA - v / AWS) \quad (13)$$

The induced drag then calculates from

$$D_{ind} = L v / AWS \quad (14)$$

The bound vorticity of the profile is calculated from the lift per span length due to (1)

$$\Gamma_{bound} = \frac{L}{\rho AWS} \quad (15)$$

Since vorticity of free vortex filament depends on vorticity of bound vortex filament, which in turn depends on lift, itself depending on free vortex filament vorticity due to induced wind, this procedure is iterative by nature.

For a wing of finite span with varying lift distribution over span the iterative procedure is:

- (1) Assume $v=0$
- (2) Calculate profile lift per span from (13) for a given geometric angle of attack, flow speed and chord length. Additional parameters like a flap angle can be taken into account here.
- (3) Calculate Γ_{bound} over span from profile lift from (15)
- (4) Calculate v from (12) and (9)
- (5) redo 2.-5. until v converges
- (6) calculate induced drag
- (7) calculate total drag by adding parasitic profile drag to induced drag

Discretization

Generally this method allows for an arbitrary number of wings and sails in any combination as long as it is taken care that geometry and free vortex filaments do not intersect. Here we focus on the combination of a wing with a hinged flap and a jib as they are used for the AC class catamarans..

The envelope of a wing or a sail is discretized with an arbitrary number of horizontal profiles, numbered $i=1,2,\dots,N$. Each profile is described by its z -coordinate z_i along with leading and trailing edge x - and y -coordinates:

$$\mathbf{l}_i = \{x_{li}, y_{li}, z_i\} \text{ and } \mathbf{t}_i = \{x_{ti}, y_{ti}, z_i\} \quad (16)$$

In addition, for each profile an individual incident flow speed AWS_i , an incident (geometric) angle of attack AoA_i , a lift coefficient c_{Li} and a parasitic profile drag coefficient c_{DPPi} has to be known. No profile geometry is needed since the property of the profile is entirely described by the lift coefficient.

Flow force coefficients c_L , c_{DPP} and can be provided by tabulated data for given AoA and additional parameters like a flap angle β_f . This approach allows taking into account profile properties from any source, being it linear or nonlinear, from inviscid or viscous calculation methods.

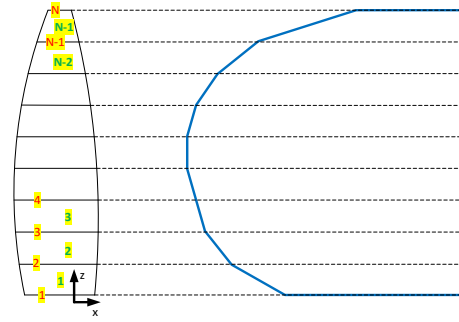


Figure 4: Discretization of wing planform

A bound vortex filament aligned with or approximately parallel to the z -axis for incident flow aligned with the x -axis is assumed. The vorticity Γ of the bound vortex filament segment between two profiles changes linearly, generating a free vortex wake sheet. At bottom profile (root) and top profile (tip) discrete free vortex filaments are generated in order to satisfy zero bound vorticity for $z < z_1$ and $z > z_N$. Consequently $\Gamma_{bound}(z)$ and $\Gamma_{fvr root}$ as well as $\Gamma_{fvr tip}$ can be calculated from profile definition information: for any profile i . $1 \leq i \leq N$:

$$\Gamma_i = 0.5 AWS_i c_i c_{Li} (AoA_i - \frac{v_i}{AWS_i}) \quad (17)$$

where the chord length is given by the distance of leading and trailing edge, $c_i = |\mathbf{t}_i - \mathbf{l}_i|$. Piecewise linear distribution of circulation and discrete circulation at the extends of the wing are defined by: for $z_i < z < z_{i+1}$

$$\Gamma_{bound}(z) = \Gamma_i + \frac{\Gamma_{i+1} - \Gamma_i}{z_{i+1} - z_i} (z - z_i) \quad (18)$$

$$\Gamma_{fvr root} = -\Gamma_1 w_{FVF} \quad (19)$$

$$\Gamma_{fvr tip} = \Gamma_N \quad (20)$$

Here w_{FVF} is a factor taking into account to which degree the root free vortex filament is suppressed by a wall. If the root of the wing is fixed to a wall without a gap, $w_{FVF}=0$. If no wall is present at all, $w_{FVF}=1$. w_{fvr} can be calculated from a known result at a particular AoA .

The end points of a bound vortex filament section within a panel is given by the quarter-points of the profiles at the lower and upper end of the panel. The quarter-point is a point on the chord of the profile 25% of the chord length from leading to trailing edge. The collocation point \mathbf{P}_j where the induced velocity is calculated in panel j - is located in the middle of the bound vortex filament section, see

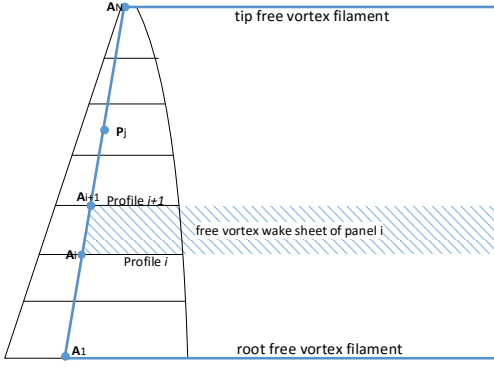


Figure 5: Bound and free vortex filaments and free vortex wake sheet due to linear change of vorticity of bound vortex filament i

For the panel i $\mathbf{A}_i = \{x_{Ai}, y_{Ai}, z_{Ai}\}^T = 0.75\mathbf{l}_i + 0.25\mathbf{t}_i$ and $\mathbf{A}_{i+1} = \{x_{Ai+1}, y_{Ai+1}, z_{Ai+1}\}^T$ are the quarter points of the lower and upper profile. $\mathbf{P}_j = \{x_{pj}, y_{pj}, z_{pj}\}^T = 0.5(\mathbf{A}_j + \mathbf{A}_{j+1})$ is the collocation point for the panel j to calculate induced velocity for the bound vortex filament segment j .

The total induced velocity in point \mathbf{P}_j is calculated by summing up the induced wind generated by any free vortex wake sheet and the discrete free vortex filaments at root and tip.

$$\begin{aligned} v_j^* = & -\frac{\Gamma_i}{4\pi} \frac{\Delta z_{root}}{\Delta y_{root}^2 + \Delta z_{root}^2} \left(1 - \frac{\Delta x_{root}}{(\Delta x_{root}^2 + \Delta y_{root}^2 + \Delta z_{root}^2)^{1/2}} \right) \\ & + \frac{\Gamma_N}{4\pi} \frac{\Delta z_{tip}}{\Delta y_{tip}^2 + \Delta z_{tip}^2} \left(1 - \frac{\Delta x_{tip}}{(\Delta x_{tip}^2 + \Delta y_{tip}^2 + \Delta z_{tip}^2)^{1/2}} \right) \\ & - \sum_{i=1}^{N-1} \frac{\Gamma_{i+1} - \Gamma_i}{4\pi(z_{i+1} - z_i)} \ln \left(\frac{\sqrt{(z_{i+1} - z_{pj})^2 + \Delta y^2 + \Delta x^2} + \Delta x}{\sqrt{(z_i - z_{pj})^2 + \Delta y^2 + \Delta x^2} + \Delta x} \right) \end{aligned} \quad (21)$$

where

$$\begin{aligned} \Delta x_{root} &= x_{A1} - x_{pj}; \quad \Delta y_{root} = y_{A1} - y_{pj}; \quad \Delta z_{root} = z_{A1} - z_{pj} \\ \Delta x_{tip} &= x_{AN} - x_{pj}; \quad \Delta y_{tip} = y_{AN} - y_{pj}; \quad \Delta z_{tip} = z_{AN} - z_{pj} \\ \Delta x &= x_{pi} - x_{pj}; \quad \Delta y = y_{pi} - y_{pj} \end{aligned} \quad (22)$$

(22) assumes $y_{Ai} = y_{Ai+1} = y_{pi}$ and $x_{Ai} = x_{Ai+1} = x_{pi}$, the latter expression only being true for a bound vortex filament parallel to the z -axis of the coordinate system. For wings of only small rake (22) is a reasonable approximation.

After calculating induced velocity in each panel, in the middle of each bound vortex filament segment, linear interpolation is used to calculate induced wind v_i at profile vertical location z_i :

$$v_i = 0.5(v_{i-1}^* + v_i^*) \quad \text{for } 2 \leq i \leq N-1 \quad (23)$$

At root and tip induced wind is calculated using linear extrapolation:

$$v_1 = 2v_1^* - v_2^* \quad (24)$$

$$v_N = 2v_{N-1}^* - v_{N-2}^* \quad (25)$$

An iterative procedure has to be used in order to calculate induced wind. We assume that for any profile i , the local height z_i , the profile length c_i , the local geometric angle of attack AoA_i and the local wind speed AWS_i is given. We also assume that lift coefficient can be calculated using the above values. Induced wind then is calculated iteratively starting with a zero guess:

- (1) Set $v_i = 0$ for any profile $i=1,2,\dots,N$
- (2) Predict profile lift coefficient $c_{Li}(AoA_i - v_i / AWS_i)$ using tabular data from 2D RANS profile solutions
- (3) Calculate Γ_i for any profile using (17)
- (4) Calculate induced wind in panel center v_C from (21)
- (5) Calculate induced wind at profile height from (23), (24) and (25)
- (6) Repeat (2) to (5) until convergence, if convergence achieved continue
- (7) Calculate lift per span for any profile using (13)
- (8) Calculate induced drag per span for any profile using (14) and add parasitic profile drag per span, taken from tabulated RANSE results
- (9) calculate driving and side force per span from trigonometric relationship
- (10) Integrate over span by trapezoidal integration

It has to be taken into account, that direct integration of lift and drag over span is not feasible since their direction changes with height due to a twisted incident wind over wing span. Hence lift and drag is transformed to driving and side forces which allow integration over span independent of local incident wind.

To achieve convergence, the iterative procedure needs under-relaxation. If k denotes the current iteration step, the induced wind is calculated as a weighted average of the result of the current and last iteration step:

$$v_i^{*k} = v_i^* \omega + v_i^{*k-1} (1 - \omega) \quad (26)$$

where v_i^* is the induced wind as calculated from (21). Some attention has to be paid to the angle of attack AoA , usually defined by the angle between incident wind and a reference line of the profile (for the profile of a symmetric main element this is its center line). The angle of incidence AoA is calculated from the apparent wind angle AWA and the local rotation of the profile, given by wing rotation and wing geometric twist. This allows taking into account the sheeting of the wing and jib, their geometric twist a twist of the incident wind.

PROFILE LIFT AND DRAG COEFFICIENTS

The lifting line algorithm as outlined above relies on profile lift and drag coefficients for the wing profile as well

as for the jib profile. For the wing profile they are predicted using planar RANSE flow investigations, while for the jib profiles standard lift and drag coefficients from literature are used.

Wing profile

The geometry of the wing is given by the AC Class Rules, see Americas Cup Race Management, 2015. The rules come with a surface description of the wing (IGES-file). For the profile investigations some simplifications are applied: a single profile at 50% of the span of the wing has been investigated at a single Reynolds number of $Rn=10^7$, corresponding to an apparent wind speed of $AWS \approx 24 \text{ m/s}$. It is generally assumed that a change of the Reynolds number by a factor of less than 10 has a negligible impact on the profile lift and drag coefficients. Figure 6 shows the profile.

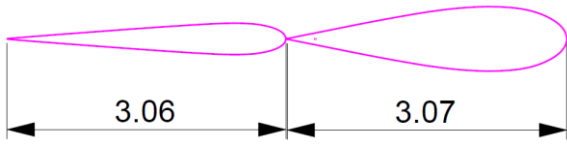


Figure 6: AC Class wing profile at 50% of wing span

Profile lift and drag coefficients are predicted using planar flow RANSE investigations. A computational grid of approximately $3 \cdot 10^5$ grid cells has been used, see Figure 7. Flow simulations have been carried out using the OpenFOAM framework, employing a solver for turbulent transient flow (pisofoam) and the SST turbulence model, see *Menter, 1994*. Intensive grid sensitive studies and validation investigation have been carried out in *Graf et.al, 2014*, hence only the main results of the wing profile study are shown here.

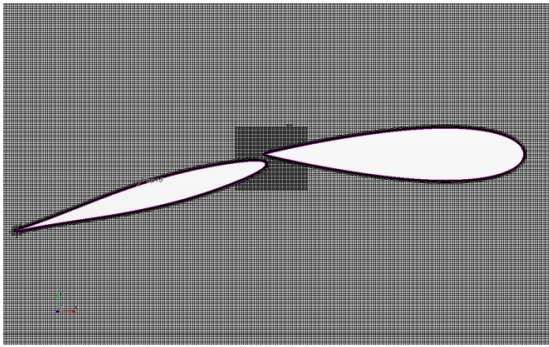


Figure 7: Computational Grid for planar flow around wing profile

A test matrix of combinations of angle of attack AoA and flap angle β has been investigated:

- 14 AoA with dense distribution of angles close to maximum lift
- 4 flap angles ranging from 0° to 30°

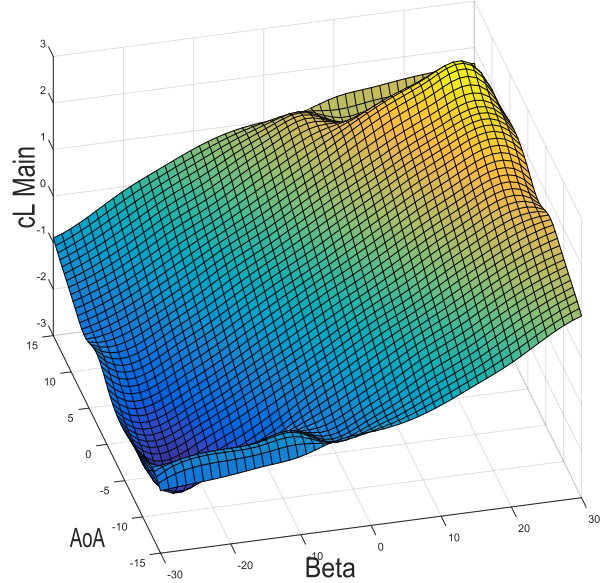


Figure 8: Wing profile lift coefficient

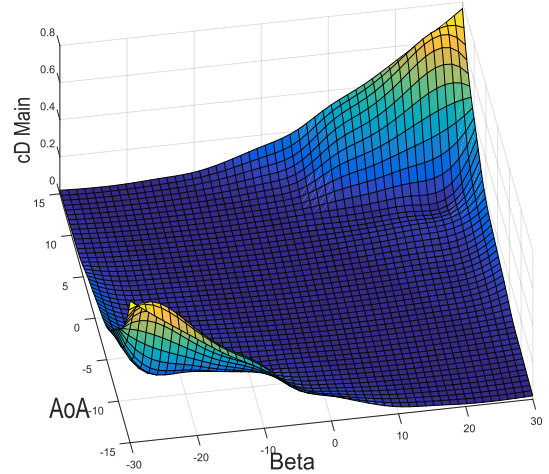


Figure 9: Wing profile drag over lift coefficient

Jib Profile

For the study presented here only minor attention has been paid to proper prediction of the forces generated by a jib. It is generally known that the jib only marginally contributes to the driving force of a catamaran equipped with a small jib and a large wing. The main reason for taking a jib into account was proper prediction of its impact on the incident wind and optimal trim settings of the wing. Hence only little effort has been used for proper prediction of the jib profile lift and drag coefficients.

The jib profile lift coefficient has been predicted for a rigid profile based on potential theory, see Trukenbrodt, 1964:

$$c_L = 2(\pi\beta + t/c) \quad (27)$$

where t/c is the relative profile depth, which has been fixed to the value $t/c=0.1$. In order to take softness of the jib fabric and flow separation into account, the lift coefficients of the rigid jib profile in ideal flow has been

manipulated: the ideal flow lift coefficient is used for angles of attack larger than the profile leading edge entrance angle and may never exceed values of $c_L=1.6$. For smaller angles of incidence the lift coefficient is linearly reduced to the value of 0 at an entrance angle of 0. The drag coefficient is predicted from ITTC 57 friction line and a drag factor of $c_{DPP} / c_L^2 = 0.1$. Figure 10 shows jib profile lift and drag over angle of attack.

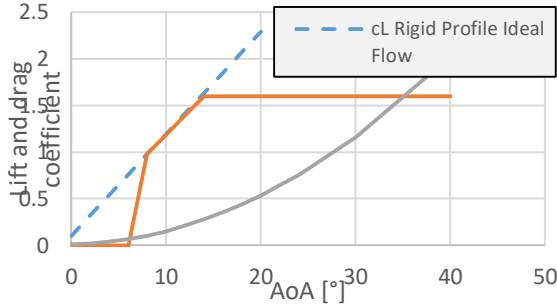


Figure 10: Coefficients of lift and parasitic profile drag of jib profile

L-FOILS AT FREE SURFACE

Geometry

L-Foils are used on sailing catamarans as daggerboard to produce side forces as well as vertical forces allowing the catamaran to fly (the hulls lift out of the water). The design of the L-foil is regarded to play a key role for the performance of any flying catamaran and intensive research is carried out to develop an optimized design. The design used for the present study is pretty much a standard design. The authors do not claim that it is an elaborated one.

The rules for the AC Class catamaran describe only little constraints on the foils: the maximum dimension is given (3.5m), the deepest point of the foil may not exceed a draft of 2.3m with respect to a measurement water plane, and there are some constraints on the maximum rotation angle around the longitudinal axis (cant axis) and the transverse axis (rake axis). Based on these constraints a simplified L-shape has been designed. It uses a NACA 64₂-010 profile, extruded along an L-shaped curved, see Figure 11.

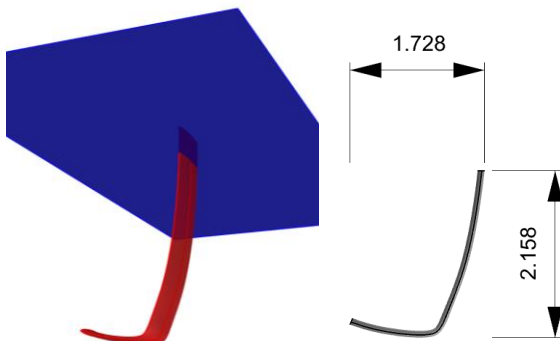


Figure 11: Water surface piercing L-shaped daggerboard

RANSE free surface flow solver

The hydrodynamic properties of the daggerboard have been investigated using a proprietary free surface RANSE code. This code has been developed based on the OpenFOAM field operation toolbox. Free surface flow simulation is based on the principle of the well-known Volume-of-Fluid-method, involving the solution of an additional conservation equation for the fluid fraction.

OpenFOAM provides solvers for the simulation of free surface flow. However these standard solvers are hardly capable to solve real world free surface flow problems with multi-million grid cells, since they lack computational efficiency and robustness. Hence a proprietary solver for free surface simulations has been developed.

Compared to the standard solvers the new solver allows large time steps, while remaining stable, thus making it possible to achieve a steady-state solution even for large computational grids within reasonable computational run time. To this end the BRICS scheme has been implemented for the discretization of the convective term in the fluid fraction conservation equation. Additional modifications of the method implement special treatment of the pressure gradient in the vicinity of the free surface.

This new OpenFOAM flow solver is presented at this conference, for details of its principles and implementation please consult Meyer et.al, 2016. An intensive validation study is also given there.

Test matrix and setup

The daggerboard acts as a water-piercing foil even when it is fully submerged and the catamaran hull starts to float. When the catamaran hull's hydrostatic lift exceed a given threshold (20% of weight) the daggerboard is assumed to act fully submerged under a flat plate. In this case the flow around the daggerboard is simulated for a fully submerged daggerboard with a rigid water surface, not taking account of any wave generation. Linear blending is used between foil at free surface and foil under flat plate for hull buoyancy between 0 and 0.6 m³. This assumption is used to avoid free surface flow simulation with daggerboard and hull, which are too time-consuming to be done within this study. While this approach will model the onset of transition into flying state reasonable accurate, the process of transition will not be modelled correctly.

As a test matrix a full permutation of the following trim settings of the daggerboard has been investigated:

- Speed 6 m/s, 12 m/s and 18 m/s
- Rake angle -2°, 0° and 2°
- Leeway angle 0° and 2°
- Cant angle 0° and 15°
- Immerse 0.4, 0.7 and 1.0

This results in 108 individual daggerboard trim parameter combinations, which have investigated using the RANSE-solver. Here *Immerse* is a parameter defining the immersion of the foil at rest. *Immerse=1* is the daggerboard at maximum draft while *immerse=0* describes a daggerboard just touching the water surface. Immerse

approximately but not exactly scales with the vertical draft of the daggerboard.

The ACC rules only allow either fully down or fully retracted daggerboard positions. Hence the *immerse* factor is used to take into account lifting of the entire catamaran out of the water due to the vertical forces generated by the foils.

Flow simulations are carried out using a finite volume discretization approach for the solution of the discrete, time averaged Navier Stokes equation. The Shear Stress Transport turbulence model (Menter, 1994) is used for turbulence modelling. The solution procedure solves the transient form of the equation since the Volume-of-Fluid method as described above is inherently transient, however a steady state solution is achieved by continuing the simulation until the unsteady disturbance of the flow field has faded away.

Computational grid

Computational grids are generated for the daggerboard configurations of two cant angles and the three immerse states. Figure 12 shows the grid for a daggerboard cant angle of 15° and an immersion of 0.7. The computational grid consists of about 3.5 million grid cells. Note the grid refinement in the vicinity of the water plane, on the surface of the foil and in the wake field.

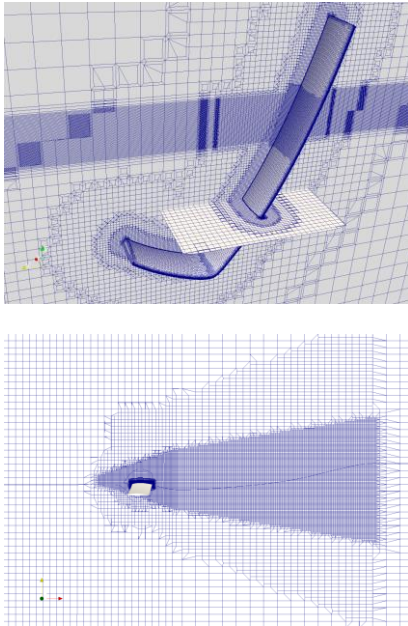


Figure 12: Computational Grid of L-foil daggerboard

ADDITIONAL RESISTANCE ELEMENTS

Additional resistance elements are hydrodynamic hull resistance, windage and rudder resistance. Only rough estimates are used for these resistance elements and they are subject to future research activities. For the method presented here, targeting wing trim optimization, the estimates are assumed to be sufficiently accurate.

Hydrodynamic Hull Resistance

Hydrodynamic hull resistance is calculated from two parameters only: the velocity and the buoyancy. No attempt has been made to take into account the impact of leeway, heel and pitch on hull resistance. The bare hull resistance is derived from an available AC 72 hull resistance curve, scaled down to the length of $L=14.65$ m and a displacement of $\Delta=3t$, the latter assumed to be the displacement in sailing trim, see Figure 13. The resistance at displacements smaller than $3t$ R_T is calculated using:

$$R_T(\Delta) = R_T(\Delta = 3t) \left(\frac{\Delta}{3t} \right)^{2/3} \quad (28)$$

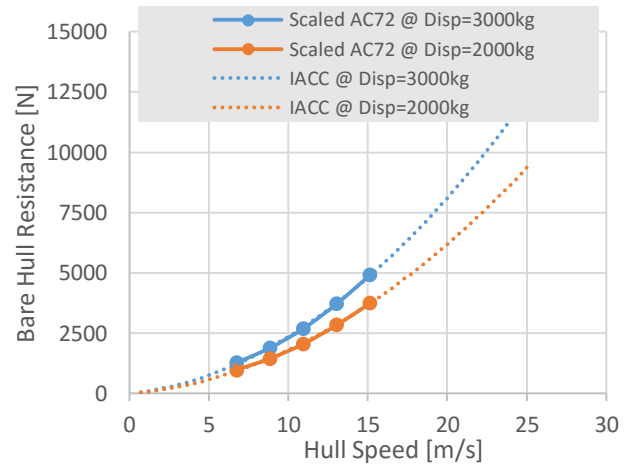


Figure 13: IACC Bare Hull Resistance

The floating displacement is calculated from the displacement at rest $\Delta=3t$ of the catamaran and the vertical lift generated by the daggerboard L_H :

$$\Delta = 3t - L_H / g \quad (29)$$

Obviously some means has to be used to avoid negative displacement.

Windage

A very simple approach is used to estimate wind resistance of the yacht's platform. Resistance in longitudinal and transverse direction are calculated from a drag area in the respective direction and the longitudinal and transverse wind speed. The drag areas are:

$$D_{AX} = 3.5 \text{ m}^2$$

$$D_{AY} = 14.5 \text{ m}^2$$

Forces in longitudinal and transverse direction are then calculated using:

$$F_{AX} = 0.5 \rho_A (AWS_{z=1m} \cos(AWA_{z=1m}))^2 D_{AX} \quad (30)$$

$$F_{AY} = 0.5 \rho_A (AWS_{z=1m} \sin(AWA_{z=1m}))^2 D_{AY} \quad (31)$$

Rudder

Rudders and rudder wings are taken into account as flat plate lifting foils, their hydrodynamic properties estimated by simple formulas derived from potential theory.

AC class rules provide values for rudder wing area and span. For the rudder itself area and span is estimated. The following values are used:

Rudder wing area:	$A_{RW}=0.18 \text{ m}^2$
Rudder wing effective span:	$S_{RW}=1.25 \text{ m}$
Rudder immersed area:	$A_R=0.28 \text{ m}^2$
Rudder effective span:	$S_R=1.4 \text{ m}$

The vertical lift of the rudder wing is calculated from

$$L_{VRW} = 0.5 \rho_H u_B^2 A_{RW} 2\pi \frac{\lambda_{RW}(\lambda_{RW} + 1)}{(\lambda_{RW} + 2)^2} \delta_{RW} \quad (32)$$

where the rudder wing aspect ratio is:

$$\lambda_{RW} = S_{RW}^2 / A_{RW} \quad (33)$$

The drag of the rudder wing is estimated from a viscous contribution, calculated from the ITTC-57 friction line and a form factor $1+k=1.3$, and from a induced drag contribution, calculated with the effective span S_{RW} :

$$R_{RW} = 0.5 \rho_H u_B^2 2A_{RW} C_{F ITTC} (1+k) + \frac{L_V^2}{S_{RW}^2 0.5 \rho_H u_B^2 \pi} \quad (34)$$

The rudder drag is calculated from a similar expression. No rudder lift is calculated since yawing moments are not taken into account in this study.

VPP-IMPLEMENTATION

The method for the calculation of boat speed is based on constrained optimization. Boat speed is maximized for the following constraints:

- Equilibrium of longitudinal aerodynamic and hydrodynamic forces and respective side forces and vertical forces.
- Heeling moment and pitching moment may not exceed given thresholds
- In addition, upper and lower bounds are given for most of the free variables of the optimization.

The free variables of the optimization are:

- Wing main element angle of attack α_M
- Wing main element twist: τ_M
- Flap angle, given at some control points over height $\beta_i = f(z_i)$
- Jib angle of attack and twist: α_J and τ_J
- Boat velocity u_B

- Leeway angle ψ
- Daggerboard immerse factor im
- Daggerboard pitch angle φ
- Daggerboard cant angle ξ
- Rudder wing angle δ_{RW}

$$\max(u_B) \quad (35)$$

subject to the following nonlinear equality and inequality constraints:

$$\sum F_x = 0 \quad (36)$$

$$\sum F_y = 0 \quad (37)$$

$$\sum F_z = 0 \quad (38)$$

$$\sum M_x \leq 135000 \text{ Nm} \quad (39)$$

$$\sum M_y \leq 100000 \text{ Nm} \quad (40)$$

and the following bounds:

$$\begin{aligned} -10 &\leq \alpha_M \leq 20 \\ 0 &\leq \tau_M \leq 5 \\ -30 &\leq \beta_i \leq 30 \\ 5 &\leq \alpha_J \leq 20 \\ 0 &\leq \tau_J \leq 15 \\ 0.4 &\leq im \leq 2 \\ -2 &\leq \varphi \leq 2 \\ 0 &\leq \xi \leq 15 \\ -3 &\leq \delta_{RW} \leq 3 \end{aligned} \quad (41)$$

As to (39) the maximum heeling moment at the break angle of the catamaran has been set to 135 kNm, which has been estimated from the yacht's main dimensions and the crew weight.

To take into account flying and non-flying states of the leeward hull, the following expression is used to calculate the total vertical force:

$$F_z = F_{Z \text{ Daggerboard}} \min(im, 1) + \max(im - 1, 0) \Delta_R g \quad (42)$$

This expression says that for $0 < im < 1$ the leeward hull is flying and the vertical force is generated entirely by the daggerboard, while for $im > 1$ the hull generates hydrostatic lift. $im=1$ indicates transition from non-flying to flying state or vice-versa while $im=2$ indicates that hydrostatic lift according to buoyancy at rest is generated.

The VPP method is implemented using the *MatLab* © programming language. For the constraint optimization a derivative-free interior point method is chosen. This method is used pretty much as a black box, so no theory is given here.

RESULTS

Comparison of wing with and without a jib

The predecessor of this publication, Graf et.al. 2014, investigated aerodynamic properties of a wing without a jib. One of the main motivations of the investigation shown here was to include a jib as it is used on an AC catamaran. So a comparison of a wing system with and without jib is of high interest.

Base of comparison has to be chosen thoroughly. Obviously a jib generates some extra driving force, but heeling moment as well and it can be assumed that it reduces the effective span of the entire system. Consequently the only reasonable comparison of wings with and without a jib is the driving force of the entire system with an optimized trim and a given heeling moment constraint. Free optimization parameters are sheeting angles and twist of the wing and the jib as well as the angle of the flap depending on height, given by four control points, distributed evenly over the wing span.

A wing similar to the one given by the new AC class rules (ACRM 2015) has been used, see right.

The span of the wing is 31.1m, the span of the jib approximately half of it.

The maximum heeling moment was set to $M_{X\ Max}=135\text{ kN}$.

The study has been carried out at a true wind speed of $TWS=8\text{m/s}$, 9m/s and 10m/s and the boat speed has been set to wind speed. True wind angle was set to $TWA=45^\circ$.

Two test cases have been studied: wing without and with a jib. For the latter case the jib sheeting has been constrained to a value where it does not curl. Figure 14 left depicts the optimized trim of the wing with the jib at $TWS=8\text{m/s}$. The jib is sheeted to an angle of approximately 10° while the main element angle is relatively open (26.7°). Without a jib, Figure 14 right, the main element is sheeted at an angle of 22.6° . The trim of the flap is almost the same for the two cases with and without a jib.

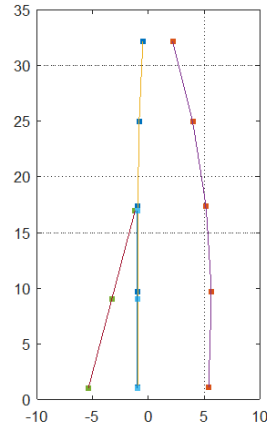


Figure 14: Trim of wing, left with jib, right no jib

Figure 15 and Figure 16 show lift coefficient of the wing and the jib over height for both test cases. The jib sheeting is set to a value with almost constant $c_{L\ Jib} \approx 1$ over its entire span, while the lift of the wing changes significantly over height, showing a maximum at approximately 1/4 of the wing height and being negative at the top, see Figure 15. When no jib is present, maximum lift of the wing is a bit higher and negative lift angles at the top are more pronounced, see Figure 16.

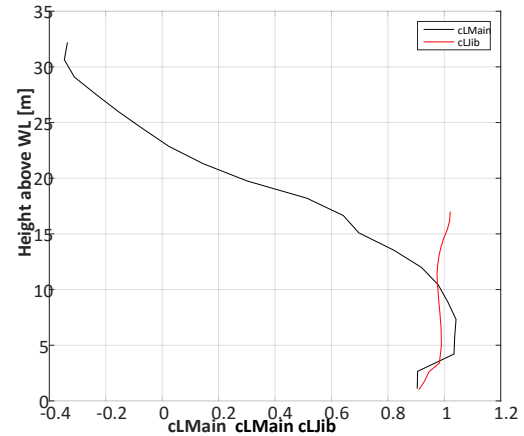


Figure 15: Lift coefficient over height for wing and close hauled jib

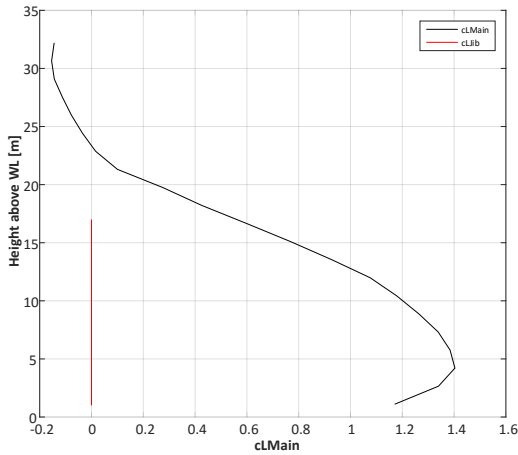


Figure 16: Lift coefficient over height for wing, no jib

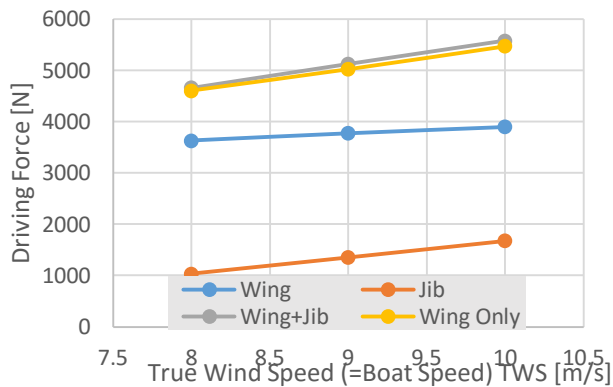


Figure 17: Driving force of wing and jib, optimized trim for heeling moment constraint

Figure 17 shows driving force of the aggregate wing with a jib and for the wing alone for optimized trim and a heeling moment constraint of $M_{X\ Max}=135\text{kN}$. While driving forces generally increase slightly with increasing wind speed, it can be seen that the jib contributes approximately 25 % to the driving force of the aggregate. However for the same heeling moment the wing without a jib can be sheeted closer, giving a driving force only slightly lower than for the aggregate. Here the difference is about 1 to 2 %. In the light of expected inaccuracy of the jib profile polar this can almost be neglected.

Free Surface Flow Simulations of Daggerboard

A single computational run took about 3 h on a single compute node with dual CPU and 24 cores. The entire test matrix has been executed in about 3 days on four nodes running parallel.

Figure 18 shows contour plots of the wave pattern for the daggerboard canted 15° at an immerse factor of 0.4 at the highest speed of 18 m/s. The wave pattern looks very different to well know wave pattern of slender hulls sailing at large Froude numbers. With a Froude number of the test case, calculated with the profile length of the daggerboard being $Fn=9$, it can be expected that the conventional

interpretation of Froude number as a speed related to the speed of a wave as long as the flow body ($Fn=0.4$) is no longer helpful.

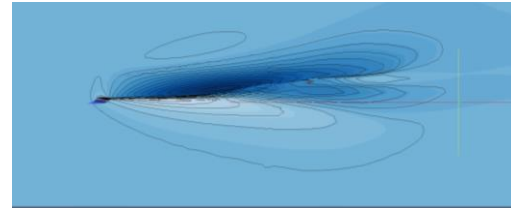
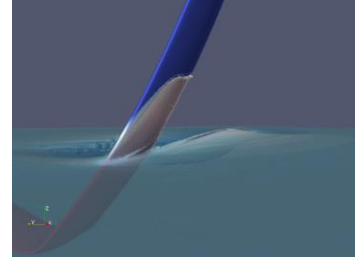


Figure 18: Wave pattern of water piercing L-foil daggerboard

Figure 19 shows total drag over total lift squared. Here total lift L is calculated from horizontal and vertical lift L_V and L_H as follows:

$$L^2 = L_H^2 + L_V^2 \quad (43)$$

The diagram shows that the simulated results can well be approximated by a straight line. It can be concluded from this, that horizontal as well as vertical lift contribute to induced drag with the same effective span. This is somewhat unexpected since the geometric span in horizontal and vertical direction differ significantly, see Figure 11.

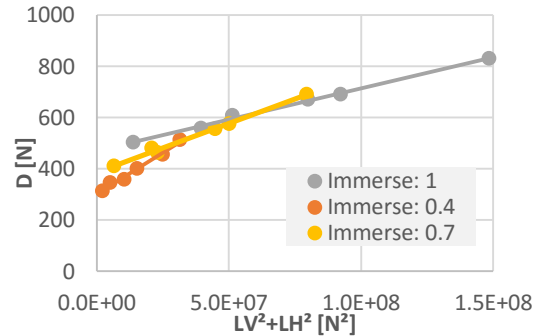


Figure 19: Drag over lift squared (cant=0°, velocity=6m/s)

Figure 20 shows horizontal lift coefficient of the daggerboard at cant angle 0° (as to Figure 11). The diagram depicts that leeway and pitch both generate horizontal lift in the same order of magnitude.

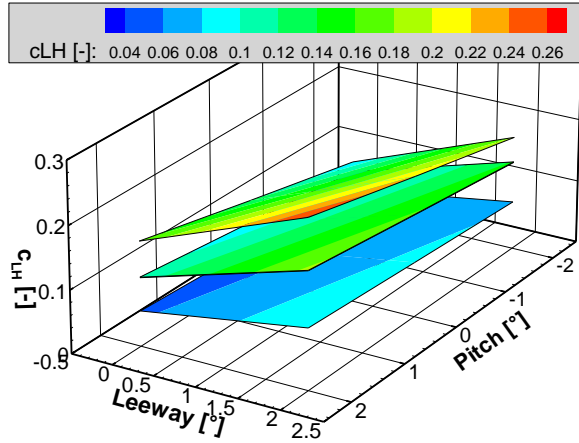


Figure 20: Daggerboard horizontal lift coefficient at cant angle 0°, plotted over pitch (rake) and leeway angle

Figure 21 shows the effective draft of the daggerboard, which is calculated from induced resistance using:

$$R_i = L^2 / (T_{\text{Eff}}^2 0.5 \rho u^2 \pi) \quad (44)$$

Two surfaces are shown in Figure 21: effective draft for cant angle 0° and 15° over immerse and velocity. These two surfaces are equidistant with a small delta between them. A clear dependency of effective draft on the immersion of the foil can be observed as expected. A slight dependency of effective draft on velocity is owed to the wave system, which also can be expected. However, the effective draft is only slightly dependent on cant angle which does not match expected behavior. It may be a consequence of the property of the foil to generate induced drag regardless whether lift is generated in horizontal or vertical direction.

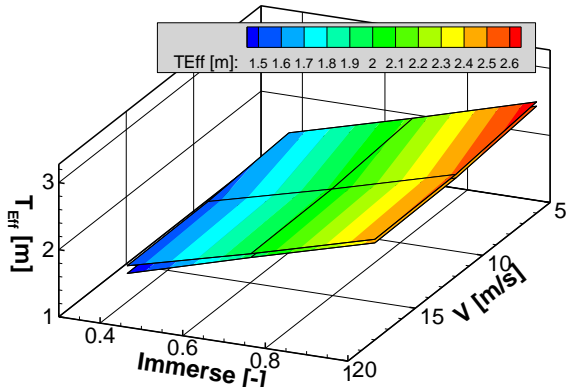


Figure 21: Effective Draft of Daggerboard at u=12m/s, two surfaces for cant angle of 0° and 15°

The hydrodynamic forces from the L-foil investigation are integrated into the VPP by a multidimensional spline-interpolated surface of the native variables (forces rather than coefficients).

Velocity Polar of AC-Catamaran

For the test case as above a velocity polar, giving boat speed and other state variables depending on true wind speed TWS and true wind angle TWA. The following test matrix has been executed:

$$6 \text{ m/s} \leq \text{TWS} \leq 11 \text{ m/s}$$

$$35^\circ \leq \text{TWA} \leq 140^\circ$$

The result of the velocity prediction is shown in Figure 22. No validation data for comparison is available and the only way for assessment of the result is a plausibility check. Generally the polar diagram shows the expected pattern. True wind angles for maximum VMG can clearly be detected and are reasonable. However the total speeds on upwind courses TWA<50° appear to be too large. For TWA=35° no reasonable results can be achieved at all. There are various possible reasons for the overestimation of speed: windage is known to have a strong impact on performance of these yachts and it is estimated only in this study. The hydrodynamic properties of the foils are predicted only up to a speed of 18m/s and are extrapolated for higher speeds. This may lead to erroneous low resistance at higher speeds.

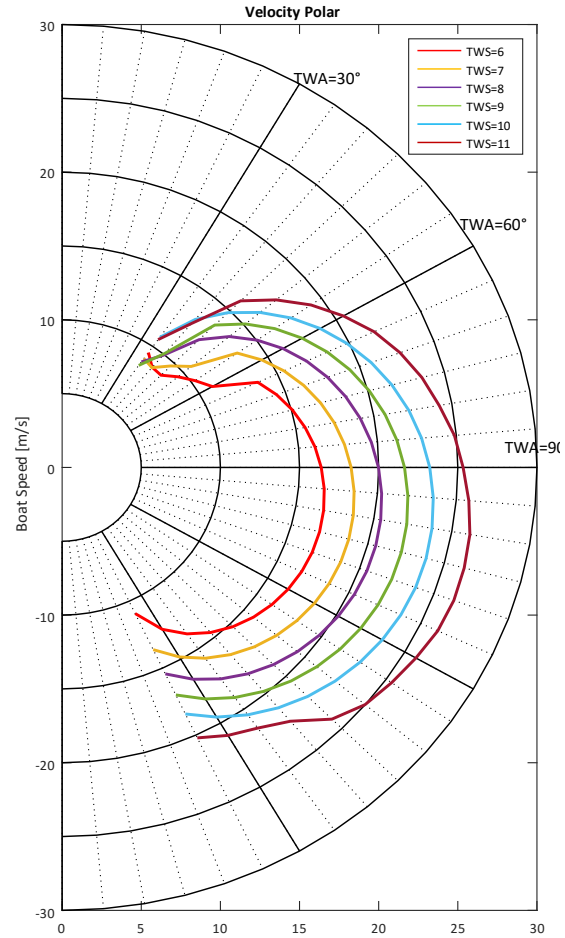


Figure 22: AC Class velocity polar

Figure 23 shows the immerse factor of the catamaran. Immerse factors below 1 indicate a flying state, while immerse factor above 1 indicate the fraction of hydrostatic lift on the entire vertical forces. The diagram depicts that for TWS=6 m/s the catamaran starts to fly at $TWA \geq 65^\circ$, while for TWS=7m/s this value is $TWA \geq 55^\circ$. For higher wind speed the catamaran flies even on the smallest true wind angles. This seems to be very optimistic and a consequence of the high velocities achieved.

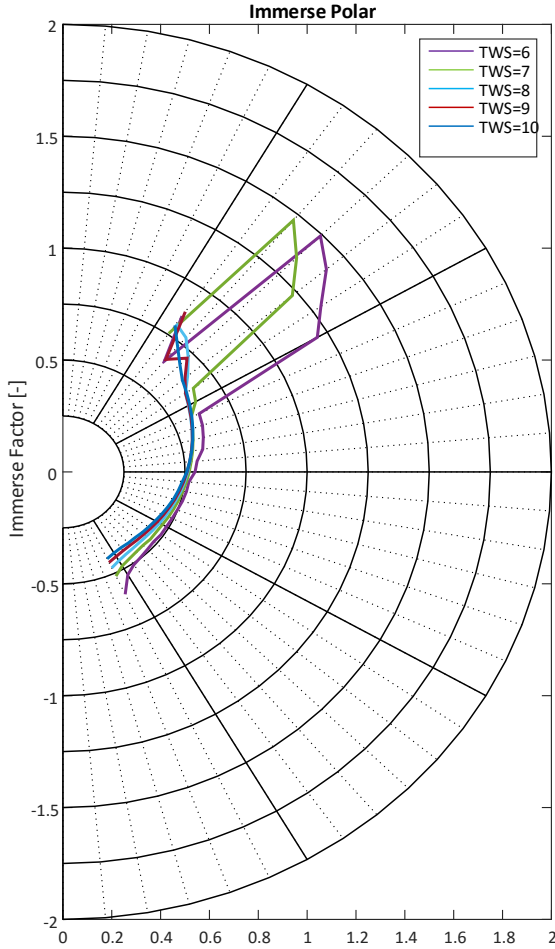


Figure 23: Polar of the immerse factor

Variation of Wind Resistance

The polars above have been generated for a drag area $D_X = 3.5 \text{ m}^2$, which is a quite low value. To assess the impact of wind resistance an additional polar has been generated with a drag area twice as high, $D_X = 7 \text{ m}^2$. Taken the beam of the platform being about 7m this is still a reasonable value.

Figure 24 shows the velocity polar for increased wind resistance. A significantly lower boat speed can be observed in particular for wind speeds $TWS \leq 8 \text{ m/s}$. Again for $TWA = 35^\circ$ no reasonable results are generated. In addition

for wind speed $TWS \geq 10 \text{ m/s}$ and $TWA \geq 70^\circ$ no useful results are generated. The iterative optimization algorithm does not converge for these wind conditions. Since the optimization solver does not completely diverge either, it is assumed that some oscillation occurs in the results, which may be caused by flat optima, however an in-depth study of the convergence behavior of the solver is beyond the scope of this study.

Figure 25 shows the immerse factor for the case of increased wind resistance. It can be clearly detected that flying of the leeward hull is postponed to higher true wind angles. At TWS=6m/s, the yacht starts to fly at $TWA \geq 70^\circ$, at TWS=7m/s this value falls to $TWA = 57^\circ$ and at TWS=8m/s flying starts at $TWA = 52^\circ$. However for TWS=9m/s the yacht flies for any investigated true wind angle, which still appears to be a bit too optimistic.

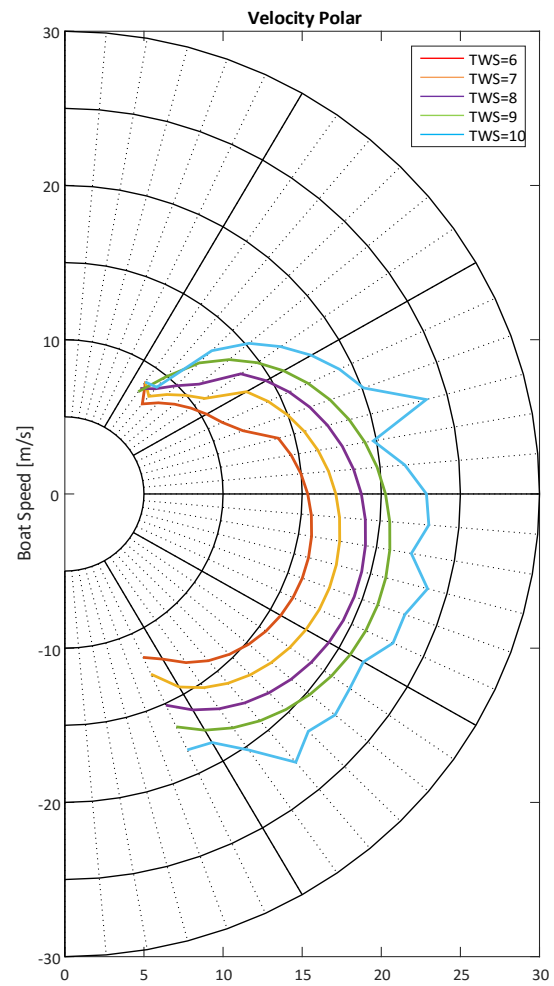


Figure 24: Velocity polar with increased wind resistance

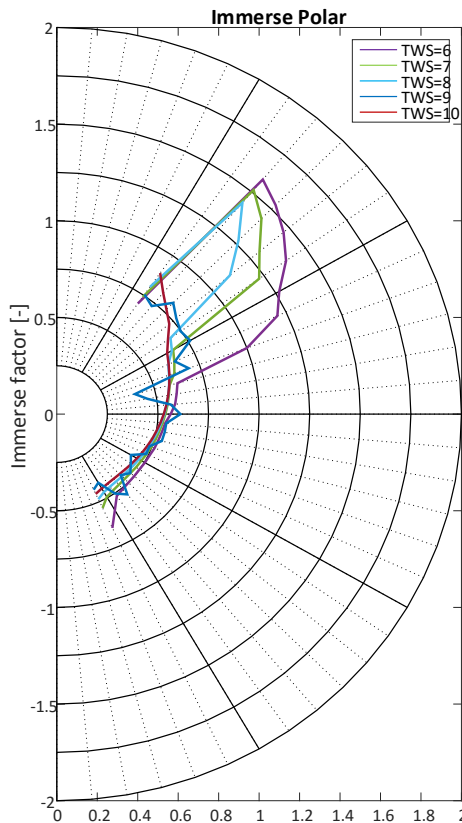


Figure 25; Polar of immerse factor, increased wind resistance

Impact of wing trim constraints

The results achieved so far have been calculated with a constraint on the wing flap restricting it to angles $-5^\circ \leq \beta \leq 30^\circ$. This results in a strong twist of the wing, with negative flap angles as well as negative lift at the top of the wing, see Figure 15. This is due to the heeling moment constraint, letting the optimizer search for a trim with a low vertical center of effort. Achieving such a large range of flap angles is not easily done in reality and needs some extra development effort of the wing builders. Consequently it is of high interest, if such high twist angles for the flap are really necessary.

The following calculations generate an excerpt of the polars, comparing the results achieved so far with a yacht with a constraint of the flap angle, restricting it to $5^\circ \leq \beta \leq 30^\circ$. This means the flap was not able to be opened as much as it has been done so far.

Figure 26 shows the result of a comparison of the speed achieved with wide bounds for the flap trim and the speed achieved with the restricted bounds for the trim of the flap. It can be seen that allowing an inversed trim of the flap gives significantly faster boat speed than a trim with no inversed flap trim. Restricting the trim of the flap to an angle larger than 5° results in a speed loss of up to 0.8m/s at TWA=95°. On an upwind tack the speed loss is about 0.5m/s, still a very large number. It can be concluded that even small changes

in the handling of the yacht can result in quite significant speed changes.

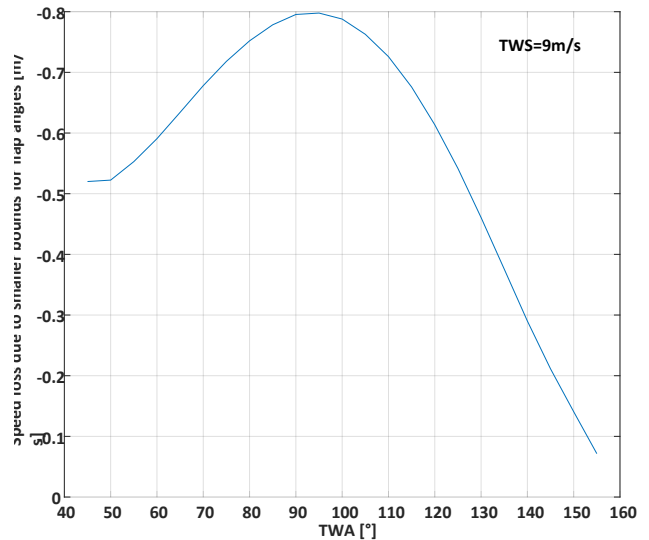


Figure 26: Speed losses due to smaller bounds for flap trimming

Conclusion

This paper presents a method for the prediction of wing generated forces on a catamaran equipped with a jib. It is combined with a hydrodynamic model for a water surface piercing daggerboard to predict the optimized trim of the wing and jib and the catamarans speed achieved with the optimized wing trim. It is demonstrated that the general approach works reasonably well and can be used to predict the optimized trim of the wing with jib and the speed of the yacht for various conditions. However much room is left for further research. The hydrodynamic model is rudimentary and needs refinement. The aerodynamic profile properties of a jib are predicted with a simplified model and the windage drag is only estimated. In addition pitching moment and heeling moment should be considered as equality rather than inequality constraint.

An additional topic of further research will be validation of the achieved results. This remains to be done after the next Americas Cup when respective data is getting available to the public.

REFERENCES

Graf, K., van Hoeve, A. and Watin, S., "Comparison of full 3D-RANS simulations with 2D-RANS/lifting line method calculations for the flow analysis of rigid wings for high performance multihulls", J Ocean Engineering,

- 2014.
- Menter, F.R., "Two-equation eddy-viscosity turbulence models for engineering applications", AIAA journal, 1994.
- Meyer, J., Renzsch, H., Graf, K. and Slawig, T., "Advanced CFD-Simulations of free-surface flows around modern sailing yachts using a newly developed OpenFOAM solver", Society of Naval and Marine Engineers, The Twenty-Second Chesapeake Sailing Yacht Symposium, Annapolis, Maryland/USA, March 2016.
- Truckenbrodt, E., Schlichting, H., „Aerodynamik des Flugzeuges: Grundlagen der Strömungsmechanik Aerodynamik des Tragflügels“ Teil 1 und 2, 2nd ed. Springer, Berlin, 1967.
- Anderson, "Fundamentals of aerodynamics", 5th ed. McGraw-Hill, Singapore, 2011
- America's Cup Race Management, America's Cup Class Rule Version 1.2, <https://drive.google.com/file/d/0B57wxyph8i5sWm1iTDNnZVU3bjA/view?pli=1>, 23rd Oct. 2015